UNCLASSIFIED

SECURITY CLASSIFICATION OF THIS PAGE (When Data Entered)

REPORT DOCUMENTATION PAGE	READ INSTRUCTIONS BEFORE COMPLETING FORM
1. REPORT NUMBER: HDL-TR-1872	2. GOVT ACCESSION NO. / 3. RECIPIENT'S CATALOG NUMBER
4. TITLE (and Subtitle): Electro-Optic Modulation of CO_2 Laser Light	5. TYPE OF REPORT & PERIOD COVERED: Technical Report
	6. PERFORMING ORG. REPORT NUMBER
7. AUTHOR(s): Dennis P. Wilkins	8. CONTRACT OR GRANT NUMBER(s): DA: 1L161102AH46H1
9. PERFORMING ORGANIZATION NAME AND ADDRESS: Harry Diamond Laboratories, 2800 Powder Mill Road, Adelphi, MD 20783	10. PROGRAM ELEMENT, PROJECT, TASK AREA & WORK UNIT NUMBERS: Program Ele: 61102A
11. CONTROLLING OFFICE NAME AND ADDRESS: Commander, US Army Electronics Command, Fort Monmouth, NJ 07703	12. REPORT DATE: December 1978
	13. NUMBER OF PAGES: 37
14. MONITORING AGENCY NAME & ADDRESS (if different from Controlling Office)	15. SECURITY CLASS. (of this report): Unclassified
	15a. DECLASSIFICATION/DOWNGRADING SCHEDULE

16. DISTRIBUTION STATEMENT (of this Report)

Approved for public release; distribution unlimited.

17. DISTRIBUTION STATEMENT (of the abstract entered in Block 20, if different from Report)

18. SUPPLEMENTARY NOTES

DRCMS Code: 611102.H.46H111
HDL Project No: 308832

19. KEY WORDS (Continue on reverse side if necessary and identify by block number)

Electro-optic
Frequency modulation
Frequency shifting
CdTe
Single-sideband

20. ABSTRACT (Continue on reverse side if necessary and identify by block number)

An experiment was performed to obtain single-sideband modulation of circularly polarized CO_2 laser radiation. The sideband was generated through the application of an effectively rotating electric field to an electro-optic crystal of cadmium-telluride through which light was passed. The theoretical basis for producing the frequency shift is presented as well as a detailed description of the experimental procedures and results. Frequency

next page

DD FORM 1 JAN 73 1473 EDITION OF 1 NOV 65 IS OBSOLETE

UNCLASSIFIED

SECURITY CLASSIFICATION OF THIS PAGE (When Data Entered)

AD A066611

163 050

50B

The findings in this report are not to be construed as an official Department of the Army position unless so designated by other authorized documents.

Citation of manufacturers' or trade names does not constitute an official indorsement or approval of the use thereof.

Destroy this report when it is no longer needed. Do not return it to the originator.

20. Abstract (Cont'd)

shifts of 200 to 500 MHz were obtained with an efficiency of 0.01 percent, and carrier-to-sideband suppression ratios up to 45 dB were achieved. Methods for improving these values are suggested which would allow the frequency-shifted signal to be used as the local oscillator in a heterodyne-detection system with state-of-the-art photovoltaic mercury-cadmium-telluride detectors.

CONTENTS

Page

1. INTRODUCTION 5

2. THEORY 6

3. EXPERIMENT 16

3.1 Laser 17

3.2 Salt Flat 17

3.3 Modulation Section 17

3.3.1 Lenses 17
3.3.2 Quarter-Wave Plates 18
3.3.3 Crystal 18
3.3.4 Power Oscillator/Quadrature Hybrid 19
3.3.5 Retardation 19
3.3.6 Polarizers 20

3.4 Detection and Diagnostics 21

3.4.1 Fabry-Perot Interferometer 21
3.4.2 Ramp 23
3.4.3 Detector 23
3.4.4 Oscilloscope 24
3.4.5 Beamsplitter 24
3.4.6 Mirror and Polarizer 24
3.4.7 Lens 24
3.4.8 Detector 25
3.4.9 Bias Circuit 26
3.4.10 Amplifier 27
3.4.11 Spectrum Analyzer 27

4. RESULTS, CONCLUSIONS, AND RECOMMENDATIONS 27

SELECTED BIBLIOGRAPHY 32

DISTRIBUTION 35

FIGURES

1 Coordinate systems in the crystal 9
2 Experimental setup 16
3 Fabry-Perot throughput 29

1. INTRODUCTION

The Harry Diamond Laboratories (HDL) has investigated single-sideband generation and frequency shifting of CO_2 laser radiation through the use of an electro-optically induced rotating birefringence.* The investigation consisted primarily of an experimental effort to demonstrate the feasibility of using electro-optically frequency-shifted radiation as a local oscillator in a CO_2 heterodyne-detection system. Such a system would contain a CO_2 laser which would be the source of radiation for both the local oscillator and the transmitted beam. Because these two signals do not vary independently in frequency, very small Doppler shifts in the return radiation could be detected in a heterodyne system. At the other extreme, Doppler shifts from very fast objects could be selectively compensated, avoiding the possibility that bandwidth or response-time limitations could blind a detector to the presence of these objects. Thus, Doppler shifts from a few hundred kilohertz to more than a gigahertz could be easily handled by a single system (from a running man to a re-entry vehicle).

Certainly the attributes of a fast, electronic frequency-shifting capability need little descriptive acclamation. The possible applications range from frequency-coded, information-carrying radiations, to optical pumps for other lasers, to devices for laser isotope separation.

The principle of using a rotating birefringence to generate a frequency shift of microwaves is well-known, and the use of electro-optic cubic crystals to produce optical frequency shifts was proposed as early as 1962. It is only recently, however, that crystals of sufficient purity, with the requisite optical and electro-optical characteristics, have become commercially available, making this process feasible. One such crystal is CdTe--a cubic crystal of the $\bar{4}3m$ class--used in the experiment reported here.

Through the application of an electric field, a rotating birefringence was electro-optically generated in the crystal, causing a portion of the circularly polarized laser light to be shifted to a single sideband. Frequency shifts of up to 500 MHz were obtained; experimental results confirmed the theoretical expectation that 0.01 percent of the incident light would be shifted in frequency by an amount equal to the frequency of the applied field. This value is, of course,

---

*Much of the work reported here was based on earlier work by S. M. Kulpa and H. P. Humphries of HDL.

a function of the crystal parameters and the field strength and was for a crystal 6 × 6 × 27 mm and an applied field strength of roughly 75 V. Carrier-to-sideband suppression ratios of about 40,000 were achieved with two polarizers, and the experiment indicated the feasibility of using such a frequency-shifted signal as the local oscillator in a heterodyne-detection system. Recommendations are presented which would sufficiently improve the power of the sideband signal to demonstrate such an application. One interesting and unanticipated conclusion of this experiment was that, while a functioning heterodyne-detection system needs a laser source which runs in the fundamental mode, it does not require one that runs single line. Multiline operation or even fast line-switching would present no problems for the system.

2. THEORY

The technique for electro-optically inducing a rotating birefringence in a crystal to generate a frequency shift can be described according to various methodologies. For our purposes, the propagation of light in a crystal is represented by the index ellipsoid:

$$\frac{x^2}{\left(\frac{\varepsilon_{11}}{\varepsilon_0}\right)} + \frac{y^2}{\left(\frac{\varepsilon_{22}}{\varepsilon_0}\right)} + \frac{z^2}{\left(\frac{\varepsilon_{33}}{\varepsilon_0}\right)} = 1 \quad ,$$

where ε_{11}, ε_{22}, and ε_{33} are the eigenvalues of the diagonalized permittivity tensor, and ε_0 is the free space permittivity. For an arbitrary direction of propagation in the crystal, the indices of refraction in the allowed polarization directions can be found as follows. First, we determine the ellipse formed by the intersection of the index ellipsoid and a plane through the origin perpendicular to the direction of propagation. The major and minor axes of this ellipse indicate the directions of allowed polarization, and the lengths of these axes equal $2n_1$ and $2n_2$ (where n_1 and n_2 are the indices of refraction for light polarized along those axes.)

However, we apply a field to the crystal to cause a frequency shift; thus, since an applied electric field modifies the indices of refraction in a noncentrosymmetric electro-optic crystal, we must deal with an expanded form of the index ellipsoid:

$$\left(\frac{1}{n^2}\right)_1 x^2 + \left(\frac{1}{n^2}\right)_2 y^2 + \left(\frac{1}{n^2}\right)_3 z^2 + 2\left(\frac{1}{n^2}\right)_4 yz + 2\left(\frac{1}{n^2}\right)_5 xz + 2\left(\frac{1}{n^2}\right)_6 xy = 1 \quad .$$

The *changes* in the refractive indices due to the applied electric field are

$$\Delta \left(\frac{1}{n^2}\right)_i = \sum_{j=1}^{3} r_{ij} E_j \quad .$$

The change coefficients, r_{ij}, form a 6 × 3 matrix which represents the electro-optic tensor. Since the crystal used in this experiment, cadmium telluride, was a cubic crystal with point-group symmetry $\bar{4}3m$, this report considers only cubic crystals. In these crystals, the electro-optic tensor is particularly simple, having just three elements different from zero, all of which are equal:

$$r_{ij} = \begin{Bmatrix} 0 & 0 & 0 \\ 0 & 0 & 0 \\ 0 & 0 & 0 \\ r_{41} & 0 & 0 \\ 0 & r_{41} & 0 \\ 0 & 0 & r_{41} \end{Bmatrix} \quad .$$

Thus, with an applied field $\vec{E} = (E_x, E_y, E_z)$, the equation for the index ellipsoid is

$$\frac{x^2}{n_o^2} + \frac{y^2}{n_o^2} + \frac{z^2}{n_o^2} + 2r_{41}E_x yz + 2r_{41}E_y xz + 2r_{41}E_z xy = 1 \quad ,$$

where

$n_0 = 2.6$ is the zero-field index of refraction, and
$r_{41} = 6.8 \times 10^{-12}$ m/V is the applicable electro-optic coefficient.

Single-sideband generation in a cubic crystal is accomplished by propagation of light along a threefold axis of symmetry (a [111] direction or cube diagonal); the applied electric field is transverse to this direction (see fig. 1). In this experiment, the applied field was in the $[1\bar{1}0]$ and $[11\bar{2}]$ directions. However, the electro-optic tensor shown above uses cube edges for its coordinate axes (x = [100], y = [010], z = [001]). Thus, caution must be exercised to ensure that all quantities are measured with respect to the same coordinate axes. For the time being, let x', y', and z' refer to the $[1\bar{1}0]$, $[11\bar{2}]$, and [111] directions, respectively, and let x, y, and z refer to the [100], [010], and [001] directions. Then, the applied electric field can be written

$$E_{x'} = E_m \cos \omega_m t, \qquad E_{y'} = E_m \sin \omega_m t \quad ,$$

where

E_m = amplitude of the applied field, and ω_m = frequency of the applied field.

Furthermore

$$E_x = \frac{E_{x'}}{\sqrt{2}} + \frac{E_{y'}}{\sqrt{6}} = E_m \left(\frac{\cos \omega_m t}{\sqrt{2}} + \frac{\sin \omega_m t}{\sqrt{6}} \right),$$

$$E_y = \frac{-E_{x'}}{\sqrt{2}} + \frac{E_{y'}}{\sqrt{6}} = E_m \left(\frac{-\cos \omega_m t}{\sqrt{2}} + \frac{\sin \omega_m t}{\sqrt{6}} \right),$$

$$E_z = \frac{-2E_{y'}}{\sqrt{6}} = E_m \left(\frac{-2}{\sqrt{6}} \sin \omega_m t \right) \quad .$$

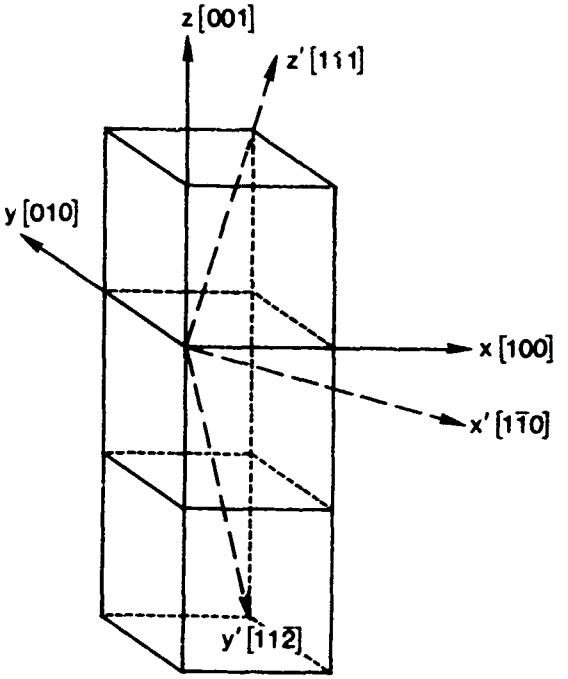

Figure 1. Coordinate systems in the crystal.

The coordinate transformations are

$$x = \frac{x'}{\sqrt{2}} + \frac{y'}{\sqrt{6}} + \frac{z'}{\sqrt{3}} \quad ,$$

$$y = \frac{-x'}{\sqrt{2}} + \frac{y'}{\sqrt{6}} + \frac{z'}{\sqrt{3}} \quad ,$$

$$z = \frac{-2y'}{\sqrt{6}} + \frac{z'}{\sqrt{3}} \quad .$$

By the use of these transformations, the equation for the index ellipsoid can be rotated to the $[1\bar{1}0], [11\bar{2}], [111]$ system of coordinate axes. With z' set equal to zero to obtain the equation of the "optical indicatrix" (the intersection of the index ellipsoid with a plane through the origin and perpendicular to the direction of propagation), we are left with the following:

$$x'^2\left(\frac{1}{n_o^2} + \frac{2r_{41}}{\sqrt{6}} E_m \sin \omega_m t\right) + y'^2\left(\frac{1}{n_o^2} - \frac{2r_{41}}{\sqrt{6}} E_m \sin \omega_m t\right)$$

$$- 2r_{41}x'y'\left(\frac{-2}{\sqrt{6}} E_m \cos \omega_m t\right) = 1 \quad .$$

To further simplify this equation and eliminate the cross term, we must do an additional rotation in the x'y' plane (henceforth, *unprimed* coordinates refer to the $[1\bar{1}0],[11\bar{2}],[111]$ system of axes). To determine the angle of rotation, consider the elliptical form

$$Ax^2 + By^2 + Cxy = 1 \quad .$$

Transforming to polar coordinates ($x = r\cos\theta$, $y = r\sin\theta$) and solving for r, we get

$$r = \left(1 - A\cos^2\theta - B\sin^2\theta - C\sin\theta\cos\theta\right)^{\frac{1}{2}} \quad .$$

Now we find the extrema in r as a function of A, B, C, and θ. This yields

$$\theta = \frac{1}{2}\arctan\left(\frac{C}{A - B}\right),$$

as the rotation needed to align the principal axes of the indicatrix with the coordinate axes.

Letting

$$A = \left(\frac{1}{n_o^2} + \frac{2}{\sqrt{6}} r_{41}E_m \sin \omega_m t\right) \quad ,$$

$$B = \left(\frac{1}{n_o^2} - \frac{2}{\sqrt{6}} r_{41}E_m \sin \omega_m t\right) \quad , \text{ and}$$

$$C = \left(4 \frac{r_{41}}{\sqrt{6}} E_m \cos \omega_m t \right) \quad ,$$

we get

$$\theta = \tfrac{1}{2}\left(\frac{\pi}{2} - \omega_m t \right) .$$

Then we rotate to a new coordinate system by making the following transformation:

$$x = x' \cos\left(\frac{\pi}{4} - \frac{\omega_m t}{2} \right) - y' \sin\left(\frac{\pi}{4} - \frac{\omega_m t}{2} \right)$$

$$y = y' \cos\left(\frac{\pi}{4} - \frac{\omega_m t}{2} \right) + x' \sin\left(\frac{\pi}{4} - \frac{\omega_m t}{2} \right) .$$

After some trigonometric simplification, we are left with the equation for the indicatrix without the cross term:

$$x'^2 \left(\frac{1}{n_o^2} + \frac{2}{\sqrt{6}} r_{41} E_m \right) + y'^2 \left(\frac{1}{n_o^2} - \frac{2}{\sqrt{6}} r_{41} E_m \right) = 1 .$$

Here, note that we are in a rotating coordinate system whose coordinate axes align with the principal axes of the (rotating) optical indicatrix. Now that we have shown that an applied electric field can electro-cptically produce a rotating birefringence, and have quantified the refractive indices for a cubic crystal like CdTe, we turn our attention to the interaction between this rotating birefringence and circularly polarized incident light.

Consider a circularly polarized electromagnetic wave incident on a crystal,

$$\vec{E}(\vec{r},t) = E_o (\hat{x} - i\hat{y}) \exp\left[i\left(\omega_o t - \vec{k} \cdot \vec{r} \right) \right]$$

where

E_o = real amplitude of the electric field,

$\hat{x},\hat{y}$ = unit vectors in the x,y directions, and

ω_o = angular frequency of the wave.

Now

$$E_x = E_o \cos\left(\omega_o t - \vec{k} \cdot \vec{r}\right) \quad ,$$

$$E_y = E_o \sin\left(\omega_o t - \vec{k} \cdot \vec{r}\right)$$

only in the nonrotating (laboratory) coordinate system. To examine what happens in the crystal, it is necessary to transform to the rotating (indicatrix) axes:

$$E_{x'} = E_x \cos\theta + E_y \sin\theta \quad ,$$

$$E_{y'} = E_y \cos\theta - E_x \sin\theta \quad ,$$

where $\theta = \frac{1}{2}(\pi/2 - \omega_m t)$ is the angle of rotation required to eliminate the cross term in the indicatrix equation. Thus,

$$E_{x'} = E_o\left[\cos\theta \cos\left(\omega_o t - \vec{k} \cdot \vec{r}\right) + \sin\theta \sin\left(\omega_o t - \vec{k} \cdot \vec{r}\right)\right] ,$$

$$E_{y'} = E_o\left[\cos\theta \sin\left(\omega_o t - \vec{k} \cdot \vec{r}\right) - \sin\theta \cos\left(\omega_o t - \vec{k} \cdot \vec{r}\right)\right],$$

or

$$E_{x'} = E_o \cos\left(\omega_o t - k_{x'} z - \theta\right) ,$$

$$E_{y'} = E_o \sin\left(\omega_o t - k_{y'} z - \theta\right) .$$

Using Maxwell's curl equations,

$$\vec{\nabla} \times \vec{E} = - \mu \frac{\partial \vec{H}}{\partial t} , \qquad \vec{\nabla} \times \vec{H} = \tilde{\varepsilon} \frac{\partial \vec{E}}{\partial t} ,$$

and setting the permeability equal to unity, we find

$$k_{x'} = \omega\sqrt{\varepsilon_{11}} = \frac{\omega_o n_{x'}}{c}$$

and

$$k_{y'} = \omega\sqrt{\varepsilon_{22}} = \frac{\omega_o n_{y'}}{c} .$$

From the elliptical form of the optical indicatrix, we set the semi-major and semi-minor axes equal to the refractive indices to get

$$n_{x'} = \left[\frac{1}{n_o^2} + \frac{2}{\sqrt{6}} r_{41} E_m\right]^{-\frac{1}{2}} ,$$

$$n_{y'} = \left[\frac{1}{n_o^2} - \frac{2}{\sqrt{6}} r_{41} E_m\right]^{-\frac{1}{2}} .$$

Since r_{41} is a very small quantity, we can put these expressions in a much more tractable form by expanding in a power series and discarding terms quadratic or higher in r_{41}. This leaves

$$n_{x'} \quad n_o - n_o^3 \frac{r_{41}}{\sqrt{6}} E_m \text{ and}$$

$$n_{y'} = n_o + n_o^3 \frac{r_{41}}{\sqrt{6}} E_m \quad .$$

Putting these expressions back in the field equations we have, finally,

$$E_{x'} = E_o \cos\left\{\omega_o\left[t - \frac{z}{c}\left(n_o - n_o^3 \frac{r_{41}}{\sqrt{6}} E_m\right)\right] - \left(\frac{\pi}{4} - \frac{\omega_m t}{2}\right)\right\} \quad ,$$

and

$$E_{y'} = E_o \sin\left\{\omega_o\left[t - \frac{z}{c}\left(n_o + n_o^3 \frac{r_{41}}{\sqrt{6}} E_m\right)\right] - \left(\frac{\pi}{4} - \frac{\omega_m t}{2}\right)\right\} \quad .$$

The phase difference at the output plane (i.e., after traversing a depth, d, of the crystal) is called the retardation, Γ; Γ is given by the difference of the trigonometric arguments above,

$$\Gamma = \omega_o \frac{2d}{c} n_o^3 r_{41} \frac{E_m}{\sqrt{6}} \quad .$$

We can write the field equations in terms of Γ:

$$E_{x'} = E_o \cos\left[\omega_o t + \frac{\Gamma}{2} - \left(\frac{\pi}{4} - \frac{\omega_m t}{2}\right) - \psi\right], \text{ and}$$

$$E_{y'} = E_o \sin\left[\omega_o t - \frac{\Gamma}{2} - \left(\frac{\pi}{4} - \frac{\omega_m t}{2}\right) - \psi\right],$$

where ψ is a common phase and is unimportant as far as frequency shifting is concerned. The final transformation to be made is a rotation back to the laboratory system at the output plane of the crystal:

$$E_x = E_{x'} \cos\theta - E_{y'} \sin\theta \quad ,$$

$$E_y = E_{y'} \cos\theta + E_{x'} \sin\theta \quad .$$

After some trigonometric manipulation, these equations can be coerced into yielding the following convenient field equations for the emerging radiation.

$$E_x = E_o \left\{\cos\frac{\Gamma}{2} \cos\omega_o t - \sin\frac{\Gamma}{2} \sin\left[\left(\omega_o + \omega_m\right)t - \frac{\pi}{2}\right]\right\}$$

$$E_y = E_o \left\{\cos\frac{\Gamma}{2} \sin\omega_o t - \sin\frac{\Gamma}{2} \cos\left[\left(\omega_o + \omega_m\right)t - \frac{\pi}{2}\right]\right\} \quad .$$

As can be seen, the original wave with positive helicity and angular frequency ω_o has now been reduced by a factor of cos $\Gamma/2$. In addition, a portion (sin $\Gamma/2$) of the wave now has opposite helicity and has been upshifted in angular frequency by an amount equal to the angular frequency of the applied field. The frequency-shifted portion of the wave will always have helicity opposite to that of the original wave and the magnitude of the frequency shift will always be equal to the frequency of the applied field. However, the direction of the shift depends on the relative helicities of the radiation and the applied field.

3. EXPERIMENT

The experimental setup is depicted schematically in figure 2; the descriptions of the equipment (sect. 3.1 to 3.4) follow the path of the radiation around that setup. It should be remembered throughout that the primary goals were to produce single-sideband radiation, suppress the unshifted radiation, and explore the feasibility of using the frequency-shifted signal as a tunable local oscillator in a heterodyne-detection system.

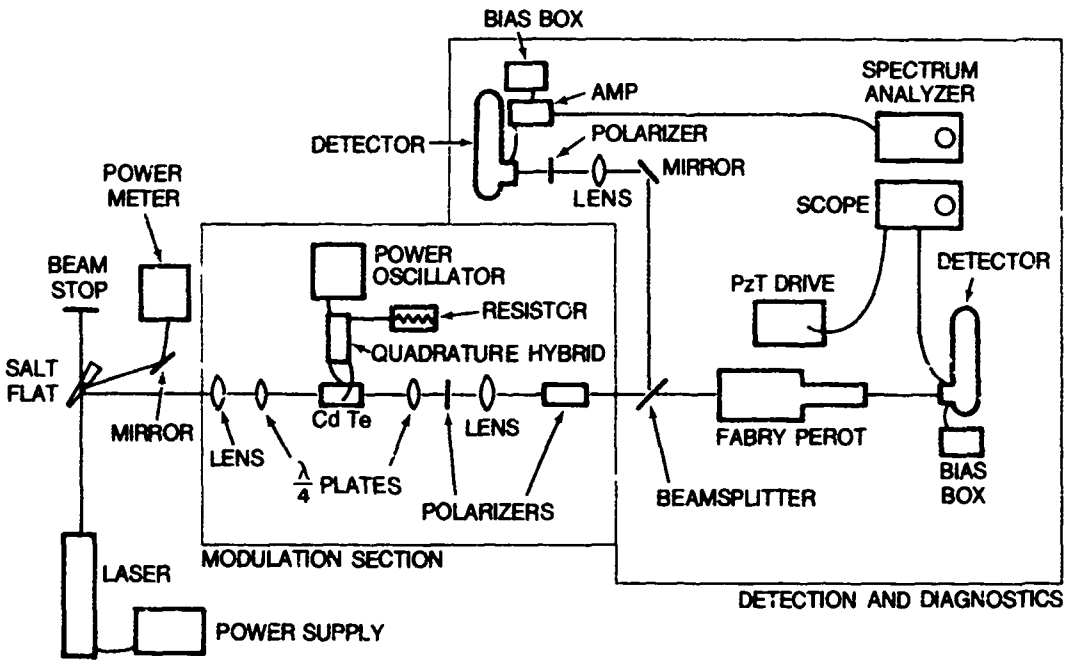

Figure 2. Experimental setup.

3.1 Laser

The source of the infrared radiation was a tunable carbon-dioxide laser with a zinc-selenide output optic, a Brewster window, and a piezoelectric tuning stack on the diffraction grating. Although the performance specifications cited by the supplier were never realized in the laboratory, some are presented here to roughly characterize the laser. It was tunable through 75 or more discrete wavelengths in the 9.17- to 10.91-μm region. It delivered at least 15 W cw power, fundamental or TEM_{00} mode, at 40 or more single wavelengths. The beam diameter was 6 mm with vertical polarization, one part in 10^9 short-term (milliseconds) frequency stability, and from 0.5- to 2-percent long-term (seconds) amplitude stability. Finally, the full angle beam divergence was quoted as less than 3 mrad.

3.2 Salt Flat

The first optical element encountered along the beam path was a salt flat used as a beamsplitter. The plane surfaces of the flat were parallel to the laser polarization, and the front surface formed an angle of $\pi/4$ with the direction of propagation--thus, ~4 percent of the incident radiation was reflected down the rail holding the optical elements. Because there was a small wedge (~4 deg) between the front and back surfaces of the flat, another beam roughly equal in power to the first could be directed continuously into a power meter for monitoring. (An incandescent light was shined on the flat to prevent cloudiness due to the hygroscopic nature of the NaCl.) The remaining ~92 percent of the laser radiation which would have been used as the transmitted beam in a functioning radar was stopped.

3.3 Modulation Section

3.3.1 Lenses

Because the transverse dimensions of the crystal were roughly the same size as the laser spot and because the applied field was uniform only near the center of the crystal, lenses were required to focus the laser light into the crystal and to recollimate it after egress. Two anti-reflection-coated, meniscus, germanium lenses were used to do this. They were coated for 10.6 μm, and had a focal length of 254 mm and a diameter of 50.8 mm.

3.3.2 Quarter-Wave Plates

Two anti-reflection-coated, cadmium-sulfide, quarter-wave plates also flanked the crystal. The first of these quarter-wave plates converted the vertically polarized laser radiation to circular polarization. The second converted the unshifted, circularly polarized radiation to horizontal polarization, and converted the frequency-shifted, circularly polarized radiation to vertical polarization. These quarter-wave plates were only 0.5 in. (1.27 cm) in diameter and were inside the pair of lenses to insure that the beam diameter was much smaller than the diameter of the quarter-wave plates.

3.3.3 Crystal

Cadmium telluride was chosen as the crystal material for this experiment because, of all available cubic electro-optic materials, it had the most desirable characteristics, including the largest $n_o^3 r_{41}$ product. It was a single crystal cut as a rectangular parallelepiped, 6 × 6 × 27 mm. The longest dimension was along [111] and the shorter dimensions were along the $[1\bar{1}0]$ and $[11\bar{2}]$ directions in the crystal. (Corners and edges were slightly beveled to inhibit chipping.) The crystal had a bulk absorptivity less than 0.002 cm^{-1} at 10.6 μm, a resistivity greater than 10^9 Ω-cm at 2 kV/cm and 60 Hz, and a breakdown voltage greater than 6 kV/cm. Two sets of silver-paint metallic electrodes were centered on the four long sides of the crystal, with each electrode measuring 4 × 27 mm. (The ends of this particular crystal were not anti-reflection coated.)

The value of the applicable CdTe electro-optic coefficient, r_{41}, was measured by the commercial providers to be 6.8×10^{-12} m/V, and this was the "clamped" crystal value. In addition to a change due to the direct electro-optic effect, the index of refraction in CdTe in the presence of an applied electric field can experience a change due to the piezoelectric effect. An alternative view is that the value of r_{41} in CdTe depends on the elastic boundary condition. At applied-field frequencies above the typical crystal resonance frequencies (~100 kHz), only the direct electro-optic effect is observed and the crystal behaves as if it were "clamped" (in a state of zero strain). In this program, both the measurement of r_{41} and experimental procedures were accomplished at higher frequencies; thus, only the direct electro-optic effect was observed.

During the experiment, the crystal was housed in a metal cylinder, which was in contact with two adjacent electrodes; this metal cylinder had three purposes. It provided shielding, acted as a heat sink for energy deposited in the crystal, and served as ground for the two contacted electrodes.

3.3.4 Power Oscillator/Quadrature Hybrid

Fields were applied to the two sets of electrodes on the long crystal faces with a power oscillator and a quadrature hybrid. The power oscillator provided from 0 to 50 W rf power at a frequency tunable from 200 to 500 MHz. The quadrature hybrid received the power from the oscillator and divided it into two equal amplitude signals one quarter cycle out of phase. These signals then left the quadrature hybrid from two separate ports and travelled along coaxial cable to the crystal electrodes. Power reflected from the electrodes back into the quadrature hybrid was deposited harmlessly through a fourth port into a 50-Ω load. Thus, in terms of voltage applied across the crystal,

$$P = \left(\frac{1}{4}\right)\frac{V^2}{R} \quad ,$$

so

$$V \approx 14\sqrt{P} \quad ,$$

where P varies from 0 to 50 W and V is in volts.

3.3.5 Retardation

It is convenient at this point to calculate what fraction of laser light would be shifted in frequency by the above-described crystal and applied voltages. Recall the retardation

$$\Gamma = \omega_o \frac{2d}{c} n_o^3 r_{41} \frac{E_m}{\sqrt{6}}$$

$$= \left(\frac{2\pi}{\lambda_o}\right)\left(\frac{2n_o^3 r_{41}}{\sqrt{6}}\right)\left(\frac{Vd}{s}\right) \quad ,$$

where

V = applied voltage,

d = crystal length = 27 mm,

s = crystal thickness = 6 mm,

λ_o = wavelength of the laser = 10.6 μm,

r_{41} = electro-optic coefficient = 6.8×10^{-12} m/V, and

n_o = index of refraction of CdTe = 2.6.

Thus

$$\sin\left(\frac{\Gamma}{2}\right) \approx \frac{\Gamma}{2} \approx 1.3 \times 10^{-4}\ V.$$

Since power goes as the square of the field amplitude,

$$P \approx 1.7 \times 10^{-8}\ V^2.$$

Thus, for an applied field of ~75 V, we see that only one part in 10^4 of the laser light is shifted in frequency.

3.3.6 Polarizers

After the light passed the crystal and the second quarter-wave plate and was again linearly polarized, it passed through two polarizers aligned so as to reject the unshifted component (horizontally polarized) and to pass the frequency-shifted component (vertically polarized). The above calculation shows that an extinction ratio of 10,000:1 would pass equal amounts of frequency-shifted and -unshifted radiation. To accomplish and exceed this, we used two polarizers. One was a wire grid on a substratum of germanium which had a functional extinction ratio of only about 7 to 8; however, it was convenient to use because it was easily rotated and its alignment properties were not especially critical. The other polarizer had an extinction ratio of 10,000:1 and passed 55 percent of the desired beam component which was reflected from a cadmium-telluride plate set at Brewster's angle. The polarization component that was transmitted by

the CdTe plate was stopped within the 15-cm cylindrical casing of the polarizer. It had a 16-mm aperture, a power handling capability of 100 W, and a wavefront distortion $<\lambda/10$; however, its alignment was critical to within a milliradian, and once it was aligned, it was seldom rotated.

3.4 Detection and Diagnostics

3.4.1 Fabry-Perot Interferometer

Since the initial setup and diagnostics were situated straight down the rail, we will not disturb the chronology of the experiment but will describe that arm of diagnostics first. The Fabry-Perot interferometer was a standard scanning interferometer. In this type of instrument with parallel mirrors, the phase difference between two emerging rays is the path difference divided by the wavelength times 2π:

$$\delta = \left(\frac{2\ell \cos\theta}{\lambda/n}\right) 2\pi \quad ,$$

where

δ = phase difference,

ℓ = mirror separation (15 cm for this experiment),

θ = angle of emergence,

n = index of refraction (for air $\sim$1), and

λ = wavelength of the light.

The reflected and transmitted light intensities can be expressed in terms of δ and the reflectance of the mirrors:

$$I_r = I_o \frac{4R \sin^2\left(\frac{\delta}{2}\right)}{(1-R)^2 + 4R \sin^2\left(\frac{\delta}{2}\right)} \qquad \text{(assuming no absorption)}$$

and

$$I_t = I_o \frac{(1 - R)^2}{(1 - R)^2 + 4R \sin^2\left(\frac{\delta}{2}\right)} ,$$

where

I_r, I_t, I_o = the reflected, transmitted, and incident light intensities and

R = reflectance of the mirrors.

Thus, we see that the maximum transmission occurs when $\delta/2 = m\pi$, where m is an integer, or

$$\delta = 2m\pi = \frac{4\pi n\ell \cos \theta}{\lambda} .$$

In terms of frequency, ν, we have

$$\nu = \frac{mc}{2n\ell \cos \theta} .$$

From this, the *free spectral range* of the instrument is defined:

$$\Delta\nu = \nu_{m+1} - \nu_m = \frac{c}{2n\ell \cos \theta} .$$

Thus, the free spectral range for our interferometer was about 1 GHz.

For a scanning interferometer, the resonance frequency varies with a small length change as follows:

$$d\nu = -\Delta\nu \frac{d\ell}{\left(\frac{\lambda}{2n}\right)} ,$$

where

$d\ell$ = incremental length change (= 5 μm) and

$d\nu$ = change in resonance frequency.

So, for our instrument parameters, the scan was over a resonance frequency range of 1 GHz--one complete free spectral range.

The interferometer throughput was exited through a 254-mm lens and pinhole attachment which allowed spatial discrimination and order selection from the interference fringe pattern.

3.4.2 Ramp

In the interferometer used for this experiment, the scan was effected with a piezoelectric drive. A linearly increasing (ramp) voltage from 0 to 1000 V was applied to three piezoelectric elements which translated the output mirror of the instrument a distance of 5 μm. This ramp voltage was also input to the oscilloscope so that other input signals could be correlated with the mirror translation and thus with the relative transmission frequency of the instrument.

3.4.3 Detector

The detector used to view the Fabry-Perot throughput was initially a copper-doped germanium photoconductor; however, the cryogenic requirements (4 K operating temperature) were excessively exacting and time-consuming for the resulting gain in sensitivity. Thus, this detector was replaced with a mercury-cadmium-telluride photodiode with $D^* > 10^{10}$ cm$\sqrt{\text{Hz}}$/W, a cutoff frequency (-3 dB) of 75 Hz, and a nominal operating temperature of 77 K. The detector was biased at 1 V and had a quantum efficiency of ~30 percent. Further information on this type of detector is presented in section 3.4.8, which discusses the detector in the other arm of optical elements.

3.4.4 Oscilloscope

The detector output was fed into a differential amplifier plug-in module for a fairly standard oscilloscope. The scope could display up to four input signals, and the standard display for this experiment was simultaneously (1) the linearly decreasing ramp voltage from the piezoelectric drive of the Fabry-Perot interferometer and (2) the signal output from the detector. An external trigger for the oscilloscope scan was taken from the ramp drive so that the two display signals were synchronized with the scan rate.

3.4.5 Beamsplitter

The beamsplitter preceding the interferometer is part of the second arm of optical elements. Made of zinc selenide, the beamsplitter was 5.08 cm in diameter and 5 mm thick. It was anti-reflection coated on the back surface so that only single-surface reflection occurred. At a 45 deg angle of incidence, the beamsplitter reflected 28 percent of light polarized perpendicular to the plane of incidence (s-polarization.)

3.4.6 Mirror and Polarizer

After being reflected from a gimbaled mirror used for alignment, the beam (containing both frequency-shifted, vertically polarized radiation and unshifted, horizontally polarized radiation) passed through another wire-grid polarizer at 45 deg which mixed the two signals. In a functioning detection system, of course, the unshifted part of this beam would be adequately suppressed, so that no detectable beat signal was produced with either the electro-optically shifted part of the beam or with the return radar signal. It was convenient in the laboratory, however, to use this unshifted portion because of its inherent collinearity with the shifted portion of the beam--a critical requirement in a heterodyne-detection system.

3.4.7 Lens

The final lens in the setup was a zinc-selenide, anti-reflection-coated meniscus lens designed for minimum spherical aberration. It had a diameter of 38 mm and a focal length of 63.5 mm. The short focal length was necessary to get as much incident power as possible onto the very small sensitive element of the detector. Other lenses were occasionally used here, including a germanium lens with a 254-mm focal length which proved to have altogether too little focusing power to be very useful.

3.4.8 Detector

This experiment required a very fast, large-bandwidth, very sensitive infrared detector. In addition, the detector could not require excessive cryogenics (liquid-helium temperatures) and still be feasible as part of a tactical system. A survey of available detectors quickly showed only one real candidate: a state-of-the-art mercury-cadmium-telluride photovoltaic detector. Accordingly, we purchased one with a 500-MHz bandwidth, $D^* = 1.3 \times 10^{10}$ cm$\sqrt{\text{Hz}}$/W, a responsivity of 2.91 A/W, and a quantum efficiency of 34 percent. The only real shortcoming of this photodiode detector was its very small sensitive area of only 1.8×10^{-4} cm^2. To drive this detector in the heterodyne mode, sufficient local oscillator power must be provided to ensure that the corresponding induced photon noise is the dominant noise source; i.e., it must be much larger than the thermal, amplifier noise.

The current produced by a local oscillator power, P_{LO}, is

$$I_{LO} = e\eta P_{LO}/h\nu \quad ,$$

where

e = electron charge,

η = quantum efficiency,

h = Planck's constant, and

ν = photon frequency,

and the noise current produced in conjunction with this is

$$I_{NLO} = \left[2eI_{LO}B\right]^{\frac{1}{2}} \qquad \text{(where B = bandwidth)},$$

$$= \left[2e^2\left(\eta P_{LO}/h\nu\right)B\right]^{\frac{1}{2}} \quad .$$

The thermal amplifier noise current that this must dominate is given by

$$I_{NT} = \left[4kTB/R_{SH}\right]^{\frac{1}{2}} ,$$

where

k = Boltzmann's constant,

T = absolute temperature,

B = bandwidth, and

R_{SH} = shunt resistance of the diode ($\simeq$ 460 Ω).

Now, setting I_{NLO} equal to 10 times I_{NT} (because of the "much larger than" requirement), we can solve for P_{LO}. Putting in the appropriate values, we find that $P_{LO} \sim 1$ mW to drive this detector in a heterodyne mode.

To bring this detector to its most sensitive operating characteristics, the following sequence should be followed. First, while the bias voltage is monitored with a VTVM, 200 mV of reverse bias is introduced on the diode. Then sufficient local oscillator power must be supplied to drive the bias voltage back to zero. Finally, the bias voltage supply should be increased until the VTVM reads between 200 and 250 mV.

3.4.9 Bias Circuit

This methodology immediately demonstrates the need for an accurately controlled, low-noise, variable-bias supply. To that end, the following circuit was designed and built.

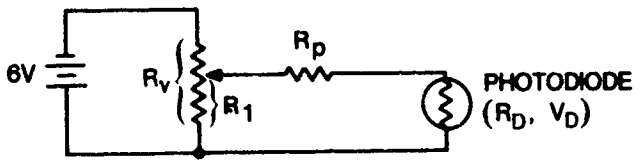

Here

R_V is a variable resistor with a total resistance of 10 kΩ,

R_p > five times the shunt resistance (or ~3 kΩ), and

R_D varies with illumination (~460 Ω at best operating point).

Now R_1 is given as a function of V_D as follows:

$$R_1 = \frac{1}{2}\left[10 - 3/V_D \pm \sqrt{(3/V_D - 10)^2 + 140}\right] \quad (R_1 \text{ is in k}\Omega).$$

Using this formula, a little computer help, and low-noise metal film resistors, we built a bias box to change the voltage across the diode in 20 increments of 25 mV each.

3.4.10 Amplifier

Because the amplifier characteristics play an integral role in determining minimum local-oscillator power and other detector operational requirements, a low-noise amplifier was designed for use with this detector. It has an internal bias "T" on the rf input which lowers the effective temperature (and hence thermal noise) seen by the detector. It has a 36-dB gain over the frequency range of 0.1 to 1.0 GHz, a 1-dB flatness, and a 3.5-dB noise figure.

3.4.11 Spectrum Analyzer

The amplifier output, consisting of one or more beat frequencies, was fed into the spectrum analyzer. This instrument resolved the input signal into its component frequencies and displayed the results on a screen. The frequency range was a function of the plug-in module used and for this experiment went from 0 to 1200 MHz.

4. RESULTS, CONCLUSIONS, AND RECOMMENDATIONS

The first obvious result of this experiment was that the source of radiation was also the source of a host of problems (one of which revealed a beneficial finding, as discussed below). Shortly after the laser's arrival, an examination of the far-field burn pattern revealed an annulus--the characteristic pattern of the (01*) mode. At the recommendation of the manufacturer, the intracavity aperture ring was reduced from the standard diameter of 8 mm. In decrements of 0.5 mm, the diameter of the ring was reduced to 4 mm. The results were reduced

power, some observable amount of unstable fundamental mode, and also some higher order modes. Finally, we replaced the original 8-mm aperture, realizing that frequent adjustments would be necessary to coerce the laser into running primarily in the fundamental mode. In this configuration, several efforts were made to measure the beam divergence. A scan of the power across the beam in the far field revealed that the intensity decreased from a central value of I_0 (power through a 1-mm hole at 3.9 m) to a value of 0.1 I_0 in a radial distance of 1 cm. This gives a full-angle beam divergence of 3.6 mrad. However, only about a third of the total laser power was contained in this central spot, which power we attribute to the fundamental mode of the laser; the remaining ~2/3 of the laser power was in higher-order modes and had a larger divergence. Further conversations with the manufacturer confirmed that the majority of their lasers of this type did not run in the fundamental mode and did not meet the power and divergence specifications.

Further experimentation revealed that the laser ran not only multimode but also multiline--this proved frustrating when we were trying to get clean pictures of the Fabry-Perot throughput. However, in the heterodyne detector, it was not a problem and may have revealed a beneficial result. The detector was much too slow to see the ~60-GHz beat between lines, and since each line had its own sideband whose beats were all in phase, the amplitudes added constructively. Thus, while a functioning heterodyne-detection system needs a laser that runs in the fundamental mode, it does not require one that runs single line; multiline operation or even fast line switching presents no problems for the system.

Figure 3 shows some of the cleanest pictures taken of the Fabry-Perot throughput as displayed on the oscilloscope. The upper trace in each picture is the voltage ramp of the Fabry-Perot piezoelectric drive. In all pictures, the peak nearest the centerline is the unextinguished (residuum after 40,000 suppression), unshifted CO_2 laser output, the peak on the right is the electro-optically produced sideband. The presence of the second (opposite) sideband visible in the $\Delta\nu$ = 200 MHz picture is due to a limitation of the quadrature hybrid used to generate the equal-amplitude, 90-deg out-of-phase applied fields. The quadrature hybrid used in this experiment had an effective lower frequency bound of ~250 MHz. Below this frequency, it fails to maintain the 90 deg phase difference between the X and Y applied fields, resulting in double sideband production. All pictures except for the $\Delta\nu$ = 500 MHz were taken with an applied transverse field of 100 V. The $\Delta\nu$ = 500 MHz picture was taken when the applied field was 75 V. The irregular shape of the peak in that picture is due entirely to the peak's proximity to the end of the Fabry-Perot piezoelectric scan.

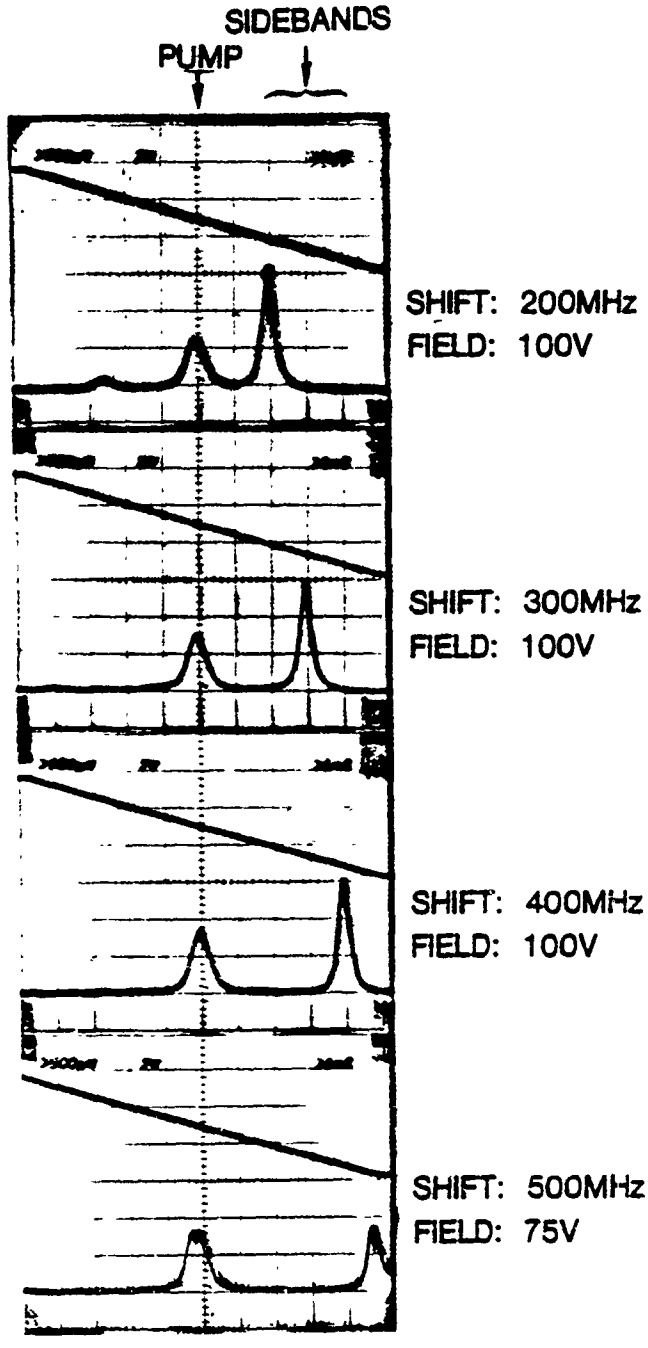

Figure 3. Fabry-Perot throughput.

In the heterodyne detector, the intermediate frequency beating at 20 and 80 MHz of the higher-order transverse modes (and even the 140-MHz longitudinal mode beating) was apparent and even proved to be useful in directing the beam onto the sensitive area of the detector. Once the beam was aligned, it quickly became apparent that there was insufficient power in the frequency-shifted signal for it to function as a local oscillator and drive the detector in a heterodyne mode. In fact, only about 2 to 3 μW of power from the shifted signal could be focused onto the detector element. This figure is based on a measurement of power that could be focused through a 0.1-mm hole and agrees with calculations using the measured laser divergence. After the amount of unshifted radiation was increased, however, mixing was accomplished and the intermediate-frequency beat signal was detected with the photodiode operating in the heterodyne mode. In excellent agreement with the earlier calculations, this heterodyning required between 0.5 and 1.0 mW of local oscillator power on the detector element. To accomplish heterodyne detection using the frequency-shifted signal as a local oscillator one could make the following corrections.

- The fundamental mode of the laser, containing roughly 8 to 9 W on the 10P20 line, could be isolated with a system of lenses, polarizers, and pinholes. Thus, instead of 0.3 W of TEM_{00} mode power hitting the crystal, up to 9 W could be used. This change would increase the frequency-shifted signal by a factor of ~27.

- A crystal with dimensions of 4 × 4 × 40 mm and anti-reflective coatings on the ends would increase the fraction of frequency-shifted radiation by a factor of ~8.

- The beamsplitter preceding the Fabry-Perot interferometer could be replaced by a mirror, increasing the frequency-shifted power at the detector by a factor of 4.

The small detector area is unavoidable as is the divergence of the laser (unless a different laser is used), but the above corrections give an improvement factor greater than 850 which would give sufficient single-sideband power in the frequency-shifted signal to allow it to function as a local oscillator. Higher applied voltages could also be employed, as well as different crystal geometries (tandem phase arrangements, cylindrical crystals, etc).

One final finding should also be mentioned. The spectrum analyzer revealed that shielding was needed, because it displayed a large signal at the applied field frequency whenever the power oscillator was functioning. Significant countermeasures were taken which reduced the problem but did not eliminate it entirely. All cables and circuits joining the equipment connected to the power oscillator or to the detector were shortened, shielded, and grounded. Further, we tried to

find the source of radiation using a directional microwave antenna. Unfortunately, because of the very weak signal strength and the probable presence of more than one source, the radiation was confirmed but not localized. In any future continuation of this experiment, plans should be made to provide better shielding to address this problem.

In conclusion, this method of generating single-sideband laser radiation demonstrates the following results in excellent agreement with the theoretical predictions. Laser radiation can be electro-optically shifted in frequency by an amount equal to the frequency of the applied field. The amount of power shifted into the sideband goes as the square of the calculated retardation. The shifted radiation exhibits a helicity opposite to that of the incident radiation, allowing the selective suppression of the carrier. A detection system using such frequency-shifted radiation as a local oscillator promises greater versatility and sensitivity than either acousto-optic systems or double-laser systems can offer.

SELECTED BIBLIOGRAPHY

F. Arams et al, 5.2-Infrared 10.6-Micron Heterodyne Detection with GHz IF Capability, IEEE J. Quantum Elect., QE-3, No. 11 (November 1967).

W. Bicknell et al, 10.6 m FM-Chirp Radar Using Narrow Band Correlation Detection, IEEE J. Quantum Elect., QE-11 (Correspondence) (June 1975).

C. F. Buhrer et al, Single-Sideband Suppressed-Carrier Modulation of Coherent Light Beams, Proc. IRE, 50 (August 1962).

C. F. Buhrer et al, Optical Frequency Shifting by Electro-Optic Effect, Appl. Physics Lett., 1, No. 2 (October 1962).

C. F. Buhrer et al, Electro-optic Light Modulation with Cubic Crystals, Appl. Opt., 2, No. 8 (August 1963).

C. F. Buhrer et al, Electro-optic Effect in Optically Active Crystals, Appl. Opt., 3, No. 4 (April 1964).

C. F. Buhrer, Single Sideband Microwave Light Modulation, Proc. IEEE (August 1964).

J. Campbell et al, Rotating Waveplate Optical Frequency Shifting in Lithium Niobate, IEEE J. Quantum Elect. QE-7, No. 9 (September 1971).

R. Carpenter, The Electro-optic Effect in Uniaxial Crystals of the Dihydrogen Phosphate Type, J. Opt. Soc. Am., 40, No. 4 (April 1950).

R. Crane, Interference Phase Measurement, Appl. Opt., 8, No. 3 (March 1969).

M. Di Domenico et al, Solid State Photodetection: A Comparison between Photodiodes and Photoconductors, Proc. IEEE (February 1964).

D. Gray et al (ed), American Institute of Physics Handbook, McGraw-Hill Book Co., New York (1957).

D. Henderson et al, A Comparison of Acousto-optic and Electro-optic Modulation at 10.6 Microns, Opt. Commun., 2, No. 5 (October 1970).

C. Huang et al, Comparison of GaAs and CdTe Crystals for High Frequency Intracavity Coupling Modulation of CO_2 Lasers, IEEE J. Quantum Elect., QE-10, No. 2 (February 1974).

C. Johnson, Electro-optic Effect in CdTe at 23.35 and 27.95 Microns, Proc. IEEE, 56 (October 1968).

R. Keyes et al, A Look at Photon Detectors, Physics Today (March 1972).

J. Kiefer et al, Electro-optic Characteristics of CdTe at 3.39 and 10.6 Microns, Appl. Physics Lett., 15 (July 1969).

J. Kiefer et al, Intracavity CdTe Modulators for CO_2 Lasers, IEEE J. Quantum Elect., QE-8, No. 2 (February 1972).

S. Kulpa et al, Single Sideband Generator for CO_2 Lasers (Abstract), 1976 Annual Meeting Opt. Soc. Am.

G. Lucovsky et al, Coherent Light Detection in Solid State Photodiodes, Proc. IEEE (January 1963).

G. Lucovsky et al, High Frequency Photodiodes, Appl. Opt., 4, No. 6, (June 1965).

J. Martin et al, Identification of Absorption Lines in Gases Used to Modulate the CO_2 Laser, IEEE J. Quantum Elect., QE-10, No. 2 (February 1974).

H. Melchior et al, Photodetectors for Optical Communication Systems, Proc. IEEE, 58, No. 10 (October 1970).

S. Namba, Electro-optical Effect of Zincblende, J. Opt. Soc. Am., 51, No. 1 (January 1961).

J. F. Nye, Physical Properties of Crystals, Oxford University Press, London (1957).

C. J. Peters, Cptical Frequency Translator Using Two Phase Modulators in Tandem, Appl. Opt., 4, No. 7 (July 1965).

A. Stein, Chirp Modulated CO_2 Waveguide Laser, IEEE J. Quantum Elect., QE-11 (Correspondence) (August 1975).

W. Wolfe, Rapid Communications, Appl. Opt., 12, No. 3 (March 1973).

A. Yariv, Introduction to Optical Electronics, Holt, Rinehart, and Winston, New York (1971).

DISTRIBUTION

DEFENSE DOCUMENTATION CENTER
CAMERON STATION, BUILDING 5
ALEXANDRIA, VA 22314
ATTN DDC-TCA (12 COPIES)

COMMANDER
USA RSCH & STD GP (EUR)
BOX 65
FPO NEW YORK 09510
ATTN LTC JAMES M. KENNEDY, JR.
CHIEF, PHYSICS & MATH BRANCH

COMMANDER
US ARMY MATERIEL DEVELOPMENT
& READINESS COMMAND
5001 EISENHOWER AVENUE
ALEXANDRIA, VA 22333
ATTN DRXAM-TL, HQ TECH LIBRARY
ATTN DRCDE, DIR FOR DEV & ENGR
ATTN DRCDMD-ST

COMMANDER
US ARMY ARMAMENT MATERIEL
READINESS COMMAND
ROCK ISLAND ARSENAL
ROCK ISLAND, IL 61299
ATTN DRSAR-LEP-L, TECHNICAL LIBRARY

COMMANDER
USA MISSILE & MUNITIONS
CENTER & SCHOOL
REDSTONE ARSENAL, AL 35809
ATT. ATSK-CTD-F

DIRECTOR
US ARMY MATERIEL SYSTEMS
ANALYSIS ACTIVITY
ABERDEEN PROVING GROUND, MD 21005
ATTN DRXSY-MP

COMMANDING OFFICER
NAVAL TRAINING EQUIPMENT CENTER
ORLANDO, FL 32813
ATTN TECHNICAL LIBRARY

DIRECTOR
DEFENSE ADVANCED RESEARCH
PROJECTS AGENCY
ARCHITECT BLDG
1400 WILSON BLVD
ARLINGTON, VA 22209

DIRECTOR
DEFENSE NUCLEAR AGENCY
WASHINGTON, DC 20305
ATTN TITL, LIBRARY

UNDER SECRETARY OF DEFENSE
FOR RES AND ENGINEERING
WASHINGTON, DC 20301
ATTN TECHNICAL LIBRARY (3C128)

OFFICE, CHIEF OF RESEARCH,
DEVELOPMENT, & ACQUISITION
DEPARTMENT OF THE ARMY
WASHINGTON, DC 20310
ATTN DAMA-ARZ-A, CHIEF SCIENTIST
DR. M. E. LASSER
ATTN DAMA-ARZ-B, DR. I. R. HERSHNER

COMMANDER
US ARMY RESEARCH OFFICE (DURHAM)
PO BOX 12211
RESEARCH TRIANGLE PARK, NC 27709
ATTN DR. ROBERT J. LONTZ
ATTN DR. CHARLES BOGOSIAN

COMMANDER
ARMY MATERIALS & MECHANICS RESEARCH
CENTER
WATERTOWN, MA 02172
ATTN DRXMR-TL, TECH LIBRARY BR

COMMANDER
NATICK LABORATORIES
NATICK, MA 01762
ATTN DRXRES-RTL, TECH LIBRARY

COMMANDER
USA FOREIGN SCIENCE & TECHNOLOGY CENTER
FEDERAL OFFICE BUILDING
220 7TH STREET NE
CHARLOTTESVILLE, VA 22901
ATTN DRXST-BS, BASIC SCIENCE DIV

DIRECTOR
USA BALLISTIC RESEARCH LABORATORY
ABERDEEN PROVING GROUND, MD 21005
ATTN DRXBR, DIRECTOR, R. EICHELBERGER
ATTN DRXBR-TB, FRANK J. ALLEN
ATTN DRDAR-TSB-S (STINFO)

COMMANDER
US ARMY COMMUNICATIONS RES
& DEV COMMAND
FORT MONMOUTH, NJ 07703
ATTN DR. HIESLMAIR
ATTN J. STROZYK
ATTN DR. E. J. TEBO
ATTN DR. R. G. BUSER
ATTN J. CHARLTON

DISTRIBUTION (Cont'd)

COMMANDER
ERADCOM TECHNICAL SUPPORT ACTIVITY
TECHNICAL LIBRARY DIV
FT. MONMOUTH, NJ 07703
ATTN DELSD-L

COMMANDER
US ARMY MOBILITY EQUIPMENT
RES & DEV COMMAND
FORT BELVOIR, VA 22060
ATTN LIBRARY

DIRECTOR
NIGHT VISION & ELECTRO-OPTICS
LABORATORY
FT. BELVOIR, VA 22060

COMMANDER
USA ELECTRONICS COMMAND
WHITE SANDS MISSILE RANGE, NM 88002
ATTN DRSEL-BL, LIBRARY

DIRECTOR
DEFENSE COMMUNICATIONS
ENGINEER CENTER
1860 WIEHLE AVE
RESTON, VA 22090
ATTN PETER A. VENA

COMMANDER
US ARMY MISSILE RESEARCH
& DEVELOPMENT COMMAND
REDSTONE ARSENAL, AL 35809
ATTN DRDMI-TB, REDSTONE SCI
INFO CENTER
ATTN DRCPM-HEL, DR. W. B. JENNINGS
ATTN DR. J. P. HALLOWES
ATTN T. HONEYCUTT

COMMANDER
EDGEWOOD ARSENAL
EDGEWOOD ARSENAL, MD 21010
ATTN SAREA-TS-L, TECH LIBRARY

COMMANDER
US ARMY ARMAMENT RES & DEV COMMAND
DOVER, NJ 07801
ATTN DRDAR-TSS, STINFO DIV

COMMANDER
USA TEST & EVALUATION COMMAND
ABERDEEN PROVING GROUND, MD 21005
ATTN TECH LIBRARY

COMMANDER
USA ABERDEEN PROVING GROUND
ABERDEEN PROVING GROUND, MD 21005
ATTN STEAP-TL, TECH LIBRARY, BLDG 305

COMMANDER
WHITE SANDS MISSILE RANGE, NM 88002
ATTN DRSEL-WL-MS, ROBERT NELSON

COMMANDER
GENERAL THOMAS J. RODMAN LABORATORY
ROCK ISLAND ARSENAL
ROCK ISLAND, IL 61201
ATTN SWERR-PL, TECH LIBRARY

COMMANDER
USA CHEMICAL CENTER & SCHOOL
FORT MC CLELLAN, AL 36201

COMMANDER
NAVAL OCEAN SYSTEMS CENTER
SAN DIEGO, CA 92152
ATTN TECH LIBRARY

COMMANDER
NAVAL SURFACE WEAPONS CENTER
WHITE OAK, MD 20910
ATTN WX-40, TECHNICAL LIBRARY

DIRECTOR
NAVAL RESEARCH LABORATORY
WASHINGTON, DC 20390
ATTN CODE 2620, TECH LIBRARY BR
ATTN CODE 5554, DR. LEON ESTEROWITZ

COMMANDER
NAVAL WEAPONS CENTER
CHINA LAKE, CA 93555
ATTN CODE 753, LIBRARY DIV

COMMANDER
AF ELECTRONICS SYSTEMS DIV
L. G. HANSCOM AFB, MA 01730
ATTN TECH LIBRARY

DEPARTMENT OF COMMERCE
NATIONAL BUREAU OF STANDARDS
WASHINGTON, DC 20234
ATTN LIBRARY

DEPARTMENT OF COMMERCE
NATIONAL BUREAU OF STANDARDS
BOULDER, CO 80302
ATTN LIBRARY

DIRECTOR
LAWRENCE RADIATION LABORATORY
LIVERMORE, CA 94550
ATTN DR. MARVIN J. WEBER
ATTN DR. HELMUT A. KOEHLER

NASA GODDARD SPACE FLIGHT CENTER
GREENBELT, MD 20771
ATTN CODE 252, DOC SECT, LIBRARY

DISTRIBUTION (Cont'd)

NATIONAL OCEANIC & ATMOSPHERIC ADM
ENVIRONMENTAL RESEARCH LABORATORIES
BOULDER, CO 80302
ATTN LIBRARY, R-51 TECH REPORTS

CARNEGIE MELLON UNIVERSITY
SCHENLEY PARK
PITTSBURGH, PA 15213
ATTN PHYSICS & EE
DR. J. O. ARTMAN

UNIVERSITY OF MICHIGAN
COLLEGE OF ENGINEERING NORTH CAMPUS
DEPARTMENT OF NUCLEAR ENGINEERING
ANN ARBOR, MI 48104
ATTN DR. CHIHIRO KIKUCHI

DIRECTOR
ADVISORY GROUP ON ELECTRON DEVICES
201 VARICK STREET
NEW YORK, NY 10013
ATTN SECTRY, WORKING GROUP D

CRYSTAL PHYSICS LABORATORY
MASSACHUSETTS INSTITUTE OF TECHNOLOGY
CAMBRIDGE, MA 02139
ATTN DR. A. LINZ
ATTN DR. H. P. JENSSEN

CENTER FOR LASER STUDIES
UNIVERSITY OF SOUTHERN CALIFORNIA
LOS ANGELES, CA 90007
ATTN DR. L. G. DE SHAZER

OFFICE OF NAVAL RESEARCH
ARLINGTON, VA 22217
ATTN DR. V. O. NICOLAI

US ARMY ELECTRONICS RESEARCH
& DEVELOPMENT COMMAND
ATTN WISEMAN, ROBERT S., DR.,
DRDEL-CT
ATTN PAO
ATTN SCALES, J., CM/CCM OFFICE

HARRY DIAMOND LABORATORIES
ATTN 00100, COMMANDER/TECHNICAL DIR/TSO
ATTN CHIEF, 00210
ATTN CHIEF, DIV 10000
ATTN CHIEF, DIV 20000
ATTN CHIEF, DIV 30000
ATTN CHIEF, DIV 40000
ATTN CHIEF, LAB 11000
ATTN CHIEF, LAB 13000
ATTN CHIEF, LAB 15000
ATTN CHIEF, LAB 22000
ATTN CHIEF, LAB 21000
ATTN CHIEF, LAB 34000
ATTN CHIEF, LAB 36000
ATTN CHIEF, LAB 47000
ATTN CHIEF, LAB 48000
ATTN RECORD COPY, 94100
ATTN HDL LIBRARY, 41000 (5 COPIES)
ATTN HDL LIBRARY, 41000 (WOODBRIDGE)
ATTN CHAIRMAN, EDITORIAL COMMITTEE
ATTN TECHNICAL REPORTS BRANCH, 41300
ATTN LEGAL OFFICE, 97000
ATTN LANHAM, C., 00210
ATTN WILLIS, B., 47400
ATTN FARRAR, R., 13500
ATTN GLEASON, T., 15400
ATTN KARAYIANIS, N., 13200
ATTN KULPA, S., 13200
ATTN LEAVITT, R., 13200
ATTN MORRISON, C., 13200
ATTN NEMARICH, J., 11130
ATTN WORTMAN, D., 13200
ATTN SATTLER, J., 13200
ATTN WEBER, B., 13200
ATTN SIMONIS, G., 13200
ATTN WILKINS, D. P. (10 COPIES)